Nuclear Instruments and Methods in Physics Research A 735 (2014) 568–573

Contents lists available at ScienceDirect

Nuclear Instruments and Methods in Physics Research A

journal homepage: www.elsevier.com/locate/nima

Evaluation of the neutron scattering cross-section for light water by molecular dynamics

Y. Abe *, T. Tsuboi, S. Tasaki

Department of Nuclear Engineering, Kyoto University, Kyotodaigaku-Katsura, Nishikyo-ku, Kyoto 615-8540, Japan

ARTICLE INFO

Article history:
Received 11 April 2013
Accepted 10 October 2013
Available online 19 October 2013

Keywords:
Neutron scattering cross-section
Light water
Molecular dynamics
Cold neutron source

ABSTRACT

The neutron scattering cross-section for light water is evaluated by means of molecular dynamics (MD) simulation for incident neutron energies from 1 μeV to 10 eV at six temperatures between 293.6 and 800 K. In the evaluation, the velocity autocorrelation functions for hydrogen and oxygen are calculated from trajectory data and used for the reconstruction of the double differential scattering cross-section. Typical results on differential and total cross-sections are presented together with experimental data. As compared with ENDF/B-VII, better agreement with experiments is found on the total cross-section below several meV. Hence, the present MD-based approach can serve for the new method of generating the thermal neutron scattering cross-section library for light water.

1. Introduction

The neutron scattering cross-section for light water is utilized extensively in neutronics analysis such as detailed design of reactor cores and practical evaluation of cold neutron sources. For such a use, a reliable data set of the neutron scattering cross-section for light water is necessary over a wide range of incident neutron energies and liquid temperatures.

The theory of thermal neutron scattering was developed by Van Hove [1] in 1950s, where the neutron scattering cross-section was represented as the Fourier transform of the space-time correlation function of the particle-density operator for the target system. However, it is difficult to get the exact form of the correlation function except for the simple systems like, say, free gases and harmonic oscillators. Thus, the neutron scattering cross-sections for various moderators have been evaluated on the basis of phenomenological models [2–5].

For neutron scattering from light water, complicated molecular motions inherent to water, such as intramolecular vibration, hindered rotation and intermolecular vibration, contribute to energy transfer of incident neutrons. Since the existing evaluated nuclear data sets are mainly intended to be used in the analysis of nuclear power reactors, consistency with experiments above thermal neutron energies is regarded as important. Therefore simple models, such as the free gas model (ENDF/B-VI [3]) and the free cluster model (JEFF-3.1 [4], ENDF/B-VII [5]), are adopted to the molecular translational motion. As a result, the evaluated nuclear data sets have a problem in reproducing the experimental results below several meV, where the molecular translational motion has significant influence on the scattering cross-section.

Although several scattering cross-section models for light water, which considered the details of molecular translational motions such as intermolecular vibration (the bending and stretching modes of the hydrogen bonds between molecules) and diffusional motion, have been developed [6–8], it is rather difficult to determine systematically all the parameters used in the model over a wide range of temperatures. Thus, to include the details of the molecular motions more briefly and systematically, the scattering cross-section for light water is evaluated by molecular dynamics (MD) simulation in the present research.

The present paper is organized as follows. Section 2 describes the method for the evaluation of the neutron scattering cross-section for light water by MD. Section 3 explains the condition and result of MD simulation. In Section 4, calculated results on both differential and total cross-sections are shown and discussed. Finally in Section 5, a few concluding remarks are mentioned.

2. Method for the evaluation of the scattering cross-section

The neutron scattering cross-section for light water is mainly dominated by large incoherent scattering from hydrogen. Thus, in the present study the scattering cross-section for light water is described by the incoherent approximation. In this approximation, the double differential scattering cross-section is written by the linear combination of the self-scattering laws for hydrogen $S_s^{\mathrm{H}}(\kappa,\omega)$ and oxygen $S_s^{\mathrm{O}}(\kappa,\omega)$ as follows:

$$\frac{\mathrm{d}^2\sigma_s}{\mathrm{d}\Omega\mathrm{d}\varepsilon}=\frac{2}{\hbar}\frac{\sigma_b^{\mathrm{H}}}{4\pi}\sqrt{\frac{E}{E_0}}S_s^{\mathrm{H}}(\kappa,\omega)+\frac{1}{\hbar}\frac{\sigma_b^{\mathrm{O}}}{4\pi}\sqrt{\frac{E}{E_0}}S_s^{\mathrm{O}}(\kappa,\omega) \quad (1)$$

* Corresponding author. Tel./fax: +81 75 383 3913.
E-mail address: yutaka_abe@nucleng.kyoto-u.ac.jp (Y. Abe).

0168-9002/$ - see front matter © 2013 Elsevier B.V. All rights reserved.
http://dx.doi.org/10.1016/j.nima.2013.10.024

where σ_b^H and σ_b^O are the bound cross-sections for hydrogen and oxygen, respectively, E_0 and E are the energies of the incident and scattered neutrons, respectively and κ and ω are the momentum and energy transfer of neutrons defined as $\hbar\kappa=\hbar|\boldsymbol{k}_0-\boldsymbol{k}|$ and $\hbar\omega=E_0-E$, respectively. Here, $\boldsymbol{k}_0$ and $\boldsymbol{k}$ are the wave vectors of the incident and scattered neutrons. The self-scattering laws for each element $S_s^X(\kappa,\omega)$ are given by the Fourier transform of the intermediate self-scattering function $F_s^X(\kappa,t)$ as below

$$S_s^X(\kappa,\omega)=\frac{1}{2\pi}\int_{-\infty}^{\infty}\mathrm{d}t e^{-i\omega t}F_s^X(\kappa,t). \tag{2}$$

Note that X denotes hydrogen or oxygen by X = H or X = O. In the present evaluation, $F_s^X(\kappa,t)$ is represented by the Gaussian approximation with the width function $\Gamma^X(t)$ as

$$F_s^X(\kappa,t)=\exp\left[-\frac{\kappa^2}{2}\Gamma^X(t)\right]. \tag{3}$$

The width function $\Gamma^X(t)$ is given by [9]

$$\Gamma^X(t)=\frac{\hbar}{m_X}\int_0^{\infty}\mathrm{d}\omega\,\frac{g^X(\omega)}{\omega}\left\{\coth\left(\frac{\hbar\omega}{2k_BT}\right)(1-\cos\,\omega t)-i\,\sin\,\omega t\right\} \tag{4}$$

where $g^X(\omega)$ is the generalized frequency distribution, k_B is the Boltzmann constant, T is the temperature of water and m_X is the mass of hydrogen or oxygen. The function $g^X(\omega)$ in Eq. (4) is determined from the real part of the velocity autocorrelation $\langle\boldsymbol{v}^X(0)\cdot\boldsymbol{v}^X(t)\rangle_T$ by

$$g^X(\omega)=\frac{4m_X}{3\pi\hbar\omega}\tanh\left(\frac{\hbar\omega}{2k_BT}\right)\int_0^{\infty}\mathrm{d}t\,\mathrm{Re}\,\langle\boldsymbol{v}^X(0)\cdot\boldsymbol{v}^X(t)\rangle_T\,\cos\,\omega t. \tag{5}$$

The notation $\langle\cdots\rangle_T$ means the thermal average over the initial states of the target system. Within the framework of the present evaluation, the dynamical property of water is embedded through the velocity autocorrelation function (VAF). Thus, once the VAF for light water is given, the scattering cross-section is reconstructed from Eqs. (1)–(5).

However, since $\langle\boldsymbol{v}^X(0)\cdot\boldsymbol{v}^X(t)\rangle_T$ derived from quantum mechanics is a complex number, it could not be identified with the VAF calculated from MD. Therefore, the following approximation is made in Eq. (5): the real part of $\langle\boldsymbol{v}^X(0)\cdot\boldsymbol{v}^X(t)\rangle_T$ is substituted for the VAF from MD $\langle\boldsymbol{v}^X(0)\cdot\boldsymbol{v}^X(t)\rangle_c$ and the classical limit $\hbar\to0$ is taken to redefine the frequency distribution $g_c^X(\omega)$ as

$$g_c^X(\omega)=\frac{2m_X}{3\pi k_BT}\int_0^{\infty}\mathrm{d}t\langle\boldsymbol{v}^X(0)\cdot\boldsymbol{v}^X(t)\rangle_c\,\cos\,\omega t. \tag{6}$$

For the calculation of the width function in Eq. (4), $g_c^X(\omega)$ is used instead of $g^X(\omega)$. Note that $g_c^X(\omega)$ satisfies the normalization condition

$$\int_0^{\infty}g_c^X(\omega)\,\mathrm{d}\omega=1 \tag{7}$$

which is verified by

$$\langle(v^X(0))^2\rangle_c=\frac{3k_BT}{m_X}. \tag{8}$$

This normalization condition ensures $\Gamma^X(t)$ to approach the free gas model in the short time limit.

3. Molecular dynamics simulation of light water

To evaluate $g_c^X(\omega)$ for light water, MD simulation is carried out. As an intermolecular potential model of water, the SPC potential with intramolecular vibration [10] is adopted in the simulation and DL_POLY [11] is used for a MD simulation code.

The condition of MD simulation is listed in Table 1. MD simulation with 216 molecules is executed under the constant volume and temperature condition. Six temperatures between 293.6 and 800 K are chosen for comparison with ENDF/B-VII and, for reference, the corresponding pressures for each condition are also shown in the Table. Note that light water is in liquid phase at temperatures between 293.6 and 600 K and in supercritical phase at 800 K. Below 600 K, the positions and velocities of molecules are calculated during a period of 100 ps with the time step interval of 0.1 fs. At 800 K, the time step interval and total simulation length are reduced, respectively, to 0.05 fs and 60 ps because of more rapid decay of the VAF.

Table 1
The condition of MD simulation.

Run No.	#1	#2	#3	#4	#5	#6
Temperature (K)	293.6	300	350	400	600	800
Density (g/cm^3)	1.0	1.0	0.97	0.94	0.66	0.08
Pressure (MPa)	0.1	0.1	0.1	1	15	25
Time step interval (fs)	0.1	0.1	0.1	0.1	0.1	0.05
Number of time steps	10^6	10^6	10^6	10^6	10^6	1.2×10^6

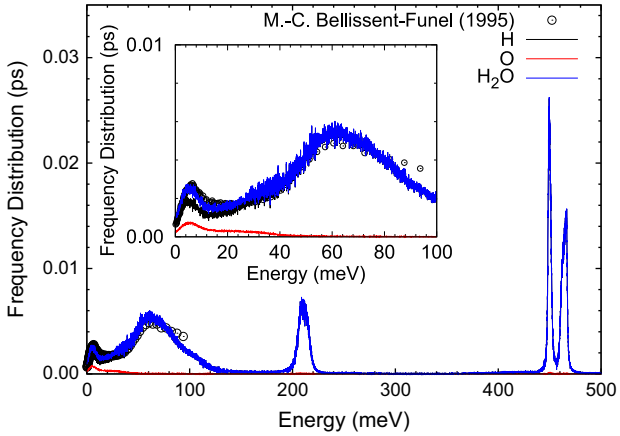

Fig. 1. Frequency distributions calculated at 300 K for H (black), O (red) and H_2O (blue) together with experimental data (circle) [12]. In the inset, spectra below 100 meV are enlarged. Note that the magnitude of experimental data, which are given in arbitrary unit, is adjusted to the height of the bending peak for H_2O. (For interpretation of the references to color in this figure caption, the reader is referred to the web version of this article.)

From trajectory data, the VAF is evaluated by

$$\langle\boldsymbol{v}^X(0)\cdot\boldsymbol{v}^X(i\Delta t)\rangle_c=\frac{1}{N_X(N_t-i)}\sum_{n=1}^{N_X}\sum_{j=0}^{N_t-i-1}\boldsymbol{v}_n^X(j\Delta t)\cdot\boldsymbol{v}_n^X(j\Delta t+i\Delta t),\quad(i=0,1,2,\ldots,N_t/2) \tag{9}$$

where Δt is the time step interval, N_t is the total number of time steps, N_X is the number of atoms for hydrogen (X=H) and oxygen (X=O) in the simulated system and $\boldsymbol{v}_n^X(j\Delta t)$ is the velocity vector of the n-th X atom at the j-th time step. Note that the maximum lag time of the VAF is reduced to half for ensuring enough sampling.

From Eq. (6), the frequency distribution is evaluated by the Fourier transform of the VAF. Fig. 1 shows the frequency distributions calculated at 300 K as a function of energy $\hbar\omega$, together with experimental data [12]. The black and red lines are the frequency distributions for hydrogen and oxygen respectively, and the blue line indicates the one for a water molecule $g_c^W(\omega)$ defined by

$$g_c^W(\omega)=\frac{2\sigma_b^Hg_c^H(\omega)+\sigma_b^Og_c^O(\omega)}{2\sigma_b^H+\sigma_b^O}. \tag{10}$$

Frequency distributions show some features inherent to liquid water i.e., for both hydrogen and oxygen, the bending (6 meV) and

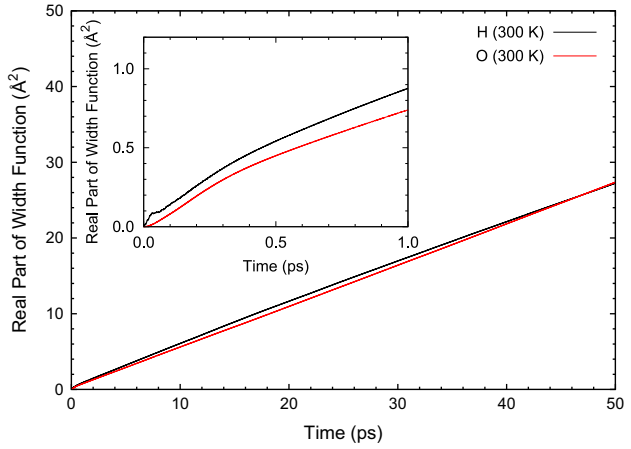

Fig. 2. Real parts of the width functions calculated at 300 K for H (black) and O (red). In the inset, the width functions below 1 ps are enlarged. (For interpretation of the references to color in this figure caption, the reader is referred to the web version of this article.)

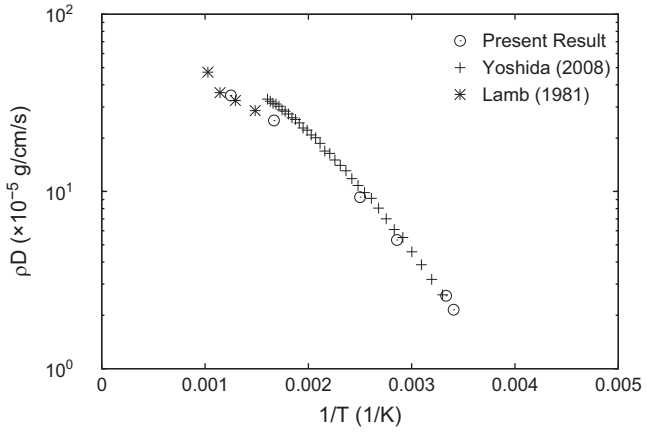

Fig. 3. Arrhenius plot of the product of diffusion coefficient D and density of water ρ together with experimental data [13,14].

stretching ($20\sim30$ meV) modes due to hydrogen bonds between molecules, and only for hydrogen, a broad peak around 60 meV due to molecular libration and three sharp peaks of the intramolecular vibration at 210, 450 and 465 meV. The calculated frequency distribution for a water molecule reasonably agrees with experimental data deduced from the neutron scattering measurement.

It should be mentioned here that according to the sampling theorem, the maximum energy $\varepsilon_{\max}$ of the frequency distribution is determined by

$$\varepsilon_{\max}=\frac{\pi\hbar}{\Delta t}. \tag{11}$$

In the present analysis, the time step intervals $\Delta t=0.1$ and 0.05 fs give $\varepsilon_{\max}=20.7$ and 41.4 eV respectively, which are high enough to evaluate the thermal neutron scattering cross-section for light water.

On the other hand, the energy interval $\Delta\varepsilon$ of the frequency distribution is determined by the data length of the VAF. As the VAF is an even function of lag time, $\Delta\varepsilon$ is given by

$$\Delta\varepsilon=\frac{2\pi\hbar}{N_t\Delta t}. \tag{12}$$

For $N_t\Delta t=100$ ps, Eq. (12) gives $\Delta\varepsilon=4.14\times10^{-2}$ meV. Thus $\Delta\varepsilon$ would restrict the minimum magnitude of energy transfer of the double differential scattering cross-section. In the present study, to evaluate the scattering cross-section below this limit, the real part of the width function is extrapolated for large lag times by the diffusion model. In Fig. 2, the real parts of the width functions for hydrogen (black) and oxygen (red) are shown as a function of lag time. Above about 10 ps, both results clearly indicate a linear relationship with t. Therefore, with diffusion coefficient D, the diffusion model

$$\mathrm{Re}\,\Gamma^{\mathrm{X}}(t)=2Dt \tag{13}$$

is applied beyond the maximum lag time. This makes possible to evaluate the scattering cross-section with small energy transfer and extends the lower limit of incident neutron energy.

To confirm the long time behavior of the calculated width function, the diffusion coefficients at the six simulated temperatures are estimated from Re $\Gamma^{\mathrm{X}}(t)$ for oxygen. In order to compare with experimental data measured on different conditions [13,14], the product of D and density of water ρ is plotted as a function of inverse temperature in Fig. 3. Including temperature dependence, the calculated results are consistent with experimental data.

4. Results and discussions

4.1. Differential cross-sections

In Figs. 4 and 5, double differential scattering cross-sections per molecule calculated at 300 K for incident neutron energy $E_0=151$ and 304 meV are shown respectively, together with experimental data [15]. To compare with experiments, calculated results are convoluted with the Gaussian resolution function. The standard deviations of the resolution function for $E_0=151$ and 304 meV are, respectively, 7.0 and 9.6 meV. In the figures, a positive sign of energy transfer ε means down-scattering.

Fig. 4 shows double differential scattering cross-sections at nine scattering angles from 15° to 165°. At 15°, a large quasielastic scattering peak is found around $\varepsilon=0$ meV. At 32°, in addition to quasielastic scattering, broad contribution of inelastic scattering also appears above about 20 meV, which is attributed to the intermolecular vibration and hindered molecular rotation found in the frequency distribution. As increasing the scattering angle, inelastic scattering becomes dominant while the magnitude of the quasielastic peak decreases and almost vanishes at 105°. Above 105°, recoil scattering from hydrogen overlaps with inelastic scattering by various molecular motions in liquid water and the width of the distribution increases at larger scattering angles. This is because the recoil energy becomes large as increasing the scattering angle while modes of the molecular motion in liquid water remain in the same energy.

In Fig. 5, double differential scattering cross-sections for $E_0=304$ meV at nine scattering angles from 15° to 140.5° are shown. In addition to the same features mentioned in Fig. 4, inelastic scattering due to the intramolecular vibration is found around $\varepsilon=210$ meV at scattering angles of 15° and 30°. At larger scattering angles above 125°, recoil scattering from hydrogen and inelastic scattering due to the molecular motions can be distinguished as different peaks. For both incident neutron energies, these features of the calculated results mentioned above are consistent with experimental data over a wide range of scattering angles.

To examine the angular distribution of scattering, differential scattering cross-sections for eight incident neutron energies from 6 to 2200 meV are calculated at 300 K and shown in Fig. 6 together with experimental data [16]. Note that in Fig. 6, the origin of each curve is shifted upward by 10 for clarity.

For an incident neutron with energy above 1 eV, hydrogen in water is approximately considered as a free atom. Thus, the angular distribution is close to a cosine curve. On the other hand,

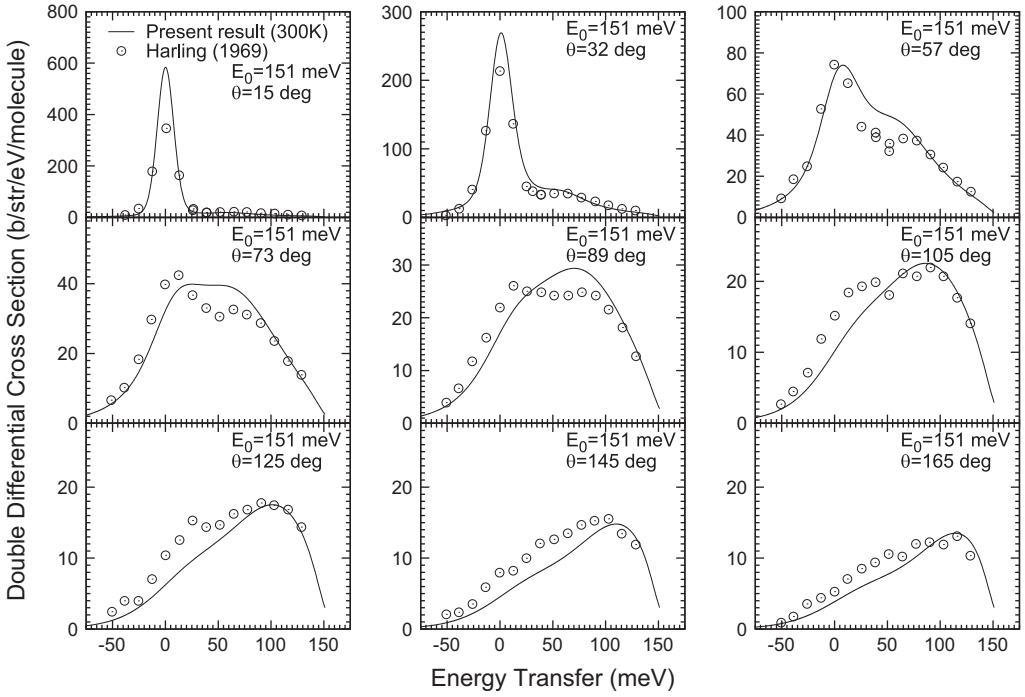

Fig. 4. Double differential cross-sections per molecule at the scattering angles θ from 15° to 165°. The solid lines indicate the calculated results at 300 K for incident neutron energy $E_0 = 151$ meV. The circles indicate experimental data [15]. Note that the calculated cross-sections are convoluted with the Gaussian resolution function with $\sigma = 7.0$ meV.

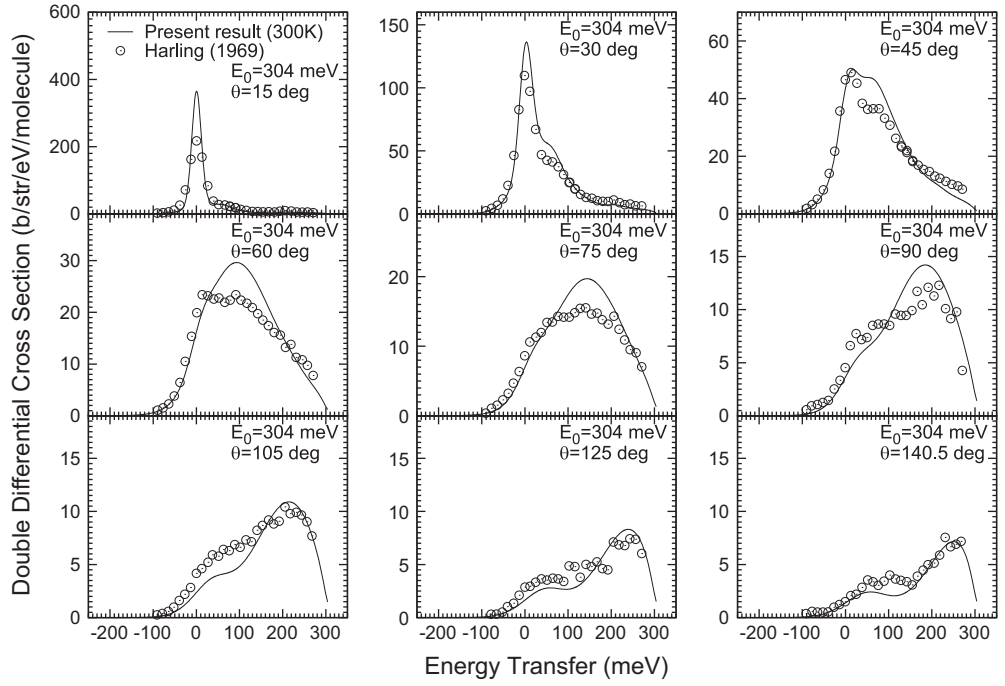

Fig. 5. Double differential cross-sections per molecule at the scattering angles θ from 15° to 140.5°. The solid lines indicate the calculated results at 300 K for incident neutron energy $E_0 = 304$ meV. The circles indicate experimental data [15]. Note that the calculated cross-sections are convoluted with the Gaussian resolution function with $\sigma = 9.6$ meV.

as decreasing incident neutron energy, the angular distribution tends to be isotropic. This is because the chemical bond in the molecule cannot be negligible and the mass of hydrogen in water increases effectively. Moreover, for the sake of large incoherent scattering by hydrogen, the angular distribution becomes structureless and information on the spatial distribution of water molecules is hardly acquired. The calculated results are in good agreement with experimental data over a wide range of incident neutron energies.

4.2. Total cross-sections

To comprehend overall behavior of the scattering cross-section for light water, the total cross-sections $\sigma_t(E_0)$ at 293.6 and 350 K

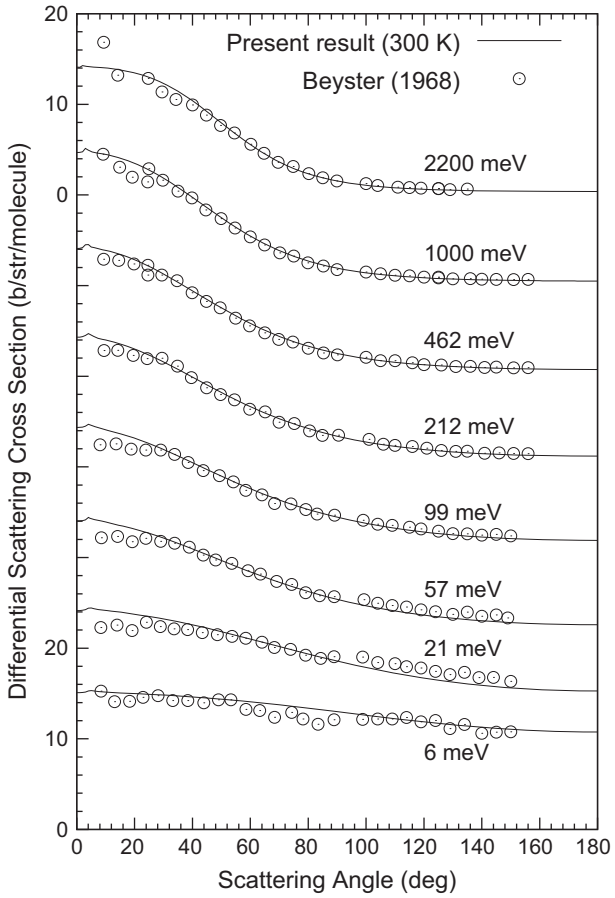

Fig. 6. Differential scattering cross-sections for incident neutron energies from 6 to 2200 meV. The solid lines indicate the calculated results at 300 K. The circles indicate experimental data [16]. Note that the origin of each curve is shifted by 10 toward the y-axis.

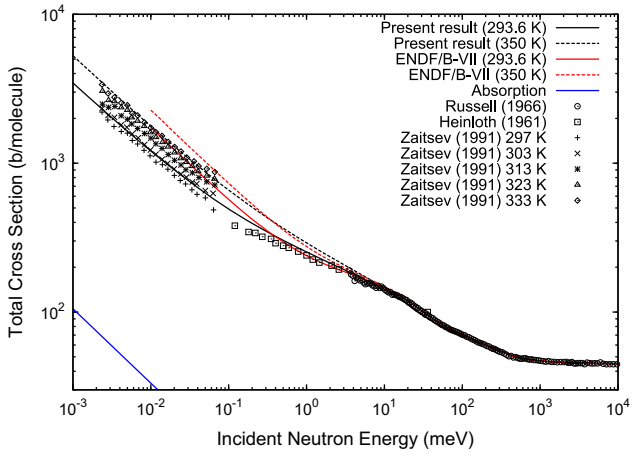

Fig. 7. Total cross-sections for light water. The black and red lines are, respectively, present results and ENDF/B-VII [5] at 293.6 and 350 K. The blue line is the absorption cross-section for light water. The symbols indicate experimental data [17–19]. (For interpretation of the references to color in this figure caption, the reader is referred to the web version of this article.)

are calculated for incident neutron energies E_0 from 1 μeV to 10 eV and shown in Fig. 7 together with ENDF/B-VII [5] and experimental data [17–19]. Assuming the $1/v$ law, the absorption cross-section for light water is also included in the calculated $\sigma_t(E_0)$ and shown in Fig. 7.

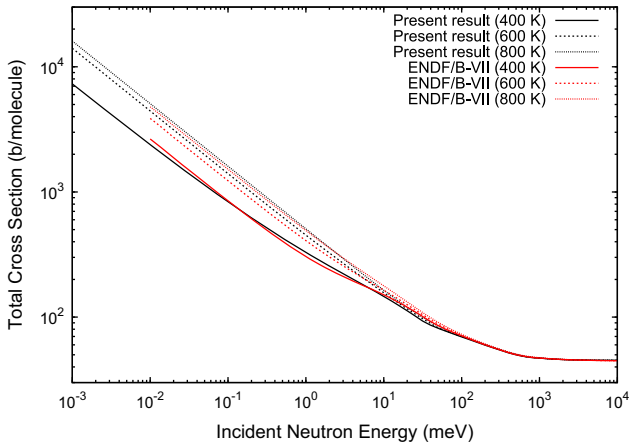

Fig. 8. Total cross-sections for light water at high temperatures. The black and red lines are, respectively, the present results and ENDF/B-VII [5]. (For interpretation of the references to color in this figure caption, the reader is referred to the web version of this article.)

The calculated results show the following features. Above 1 eV, $\sigma_t(E_0)$ approaches asymptotically to the free atom cross-section of 44.8 b. As decreasing incident neutron energy, $\sigma_t(E_0)$ increases and has a slight shoulder around 30 meV, which corresponds to the energy of the intermolecular vibration and molecular libration. Below 10 meV, $\sigma_t(E_0)$ begins to show temperature dependence since up-scattering of an incident neutron becomes dominant.

Above about 10 meV, both the present results and ENDF/B-VII agree with experimental data. Below several meV, the present results reproduce well the temperature dependence found in Zaitsev's data, while ENDF/B-VII results tend to overestimate experimental data, which would be attributed to the approximate treatment of the molecular translational motion by the free cluster model.

For further analysis, $\sigma_t(E_0)$ at 400, 600 and 800 K are calculated and shown in Fig. 8 together with ENDF/B-VII. The present results are roughly consistent with ENDF/B-VII over all incident energies since the molecular translational motion in both evaluations gets close to the free-gas-like behavior at these high temperatures.

5. Concluding remarks

In the present research, the neutron scattering cross-section for light water is evaluated by MD simulation for incident neutron energies from 1 μeV to 10 eV at six temperatures between 293.6 and 800 K. The present results agree with several experimental data at room temperatures in terms of differential and total cross-sections. In particular, the present results show improvement in the total cross-section below several meV as compared with ENDF/B-VII, which demonstrates the usefulness of MD simulation for the evaluation of the neutron scattering cross-section for light water.

As for the total cross-sections at high temperatures of 400, 600 and 800 K, comparable results are obtained in both the present and ENDF/B-VII evaluations, but some discrepancies still remain between them. To confirm the present results, comparison with experiments is necessary. However, available experimental data at these temperatures are very limited, and therefore are desired to be measured.

The present MD-based approach could also be applicable to coherent scattering since structural information such as pair distribution functions is obtainable from trajectory data. Thus, for advanced research, the evaluation of the scattering cross-section

for heavy water is now in progress and will be reported in the near future.

References

[1] L. Van Hove, Phys. Rev. 95 (1954) 249.
[2] J. Keinert, M. Mattes, JEF-1 Scattering Law Data, IKE 6-147, JEF Report 2, JEF/DOC 41.2, 1984.
[3] R.E. MacFarlane, New Thermal Neutron Scattering Files for ENDF/B-VI Release 2, Los Alamos National Laboratory Report LA-12639-MS, August 1994.
[4] M. Mattes, J. Keinert, Thermal Neutron Scattering Data for the Moderator Materials H_2O, D_2O and ZrH_x in ENDF-6 Format and as ACE Library for MCNP(X) Codes, IAEA Report INDC(NDS)-0470, April 2005.
[5] M.B. Chadwick, et al., Nucl. Data Sheets 107 (2006) 2931.
[6] N. Morishima, Y. Aoki, Ann. Nucl. Energy 22 (1995) 147.
[7] Y. Edura, N. Morishima, Nucl. Instrum. Method A 534 (2004) 531.
[8] A.D. Viñales, J. Dawidowski, J.I. Márquez Damián, Ann. Nucl. Energy 38 (2011) 1687.
[9] I.I. Gurevich, L.V. Tarasov, Low-Energy Neutron Physics, North-Holland, Amsterdam, 1968.
[10] L.X. Dang, B.M. Pettitt, J. Phys. Chem. 91 (1987) 3349.
[11] W. Smith, C.W. Yong, P.M. Rodger, Mol. Simul. 28 (2002) 385.
[12] M.-C. Bellissent-Funel, S.H. Chen, J.-M. Zanotti, Phys. Rev. E 51 (1995) 4558.
[13] K. Yoshida, N. Matubayasi, M. Nakahara, J. Chem. Phys. 129 (2008) 214501.
[14] W.J. Lamb, G.A. Hoffman, J. Jonas, J. Chem. Phys. 74 (1981) 6875.
[15] O.K. Harling, J. Chem. Phys. 50 (1969) 5279.
[16] J.R. Beyster, Nucl. Sci. Eng. 31 (1968) 254.
[17] K.N. Zaitsev, V.N. Petrov, S.P. Kuznetsov, O.A. Langer, I.V. Meshkov, A.D. Perekrestenko, Sov. At. Energy 70 (1991) 238.
[18] K. Heinloth, Z. Phys. 163 (1961) 218.
[19] J.L. Russell Jr., J.M. Neill, J.R. Brown, Total Cross Section Measurements of H_2O, General Atomic Report GA-7581, 1966.